(4)

ARL-STRUC-R-435 AR-005-570

DEPARTMENT OF DEFENCE

DEFENCE SCIENCE AND TECHNOLOGY ORGANISATION

AERONAUTICAL RESEARCH LABORATORY

MELBOURNE, VICTORIA

Aircraft Structures Report 435

ANALYSIS AND REPAIR OF IMPACT DAMAGED COMPOSITES (U)

by

J. PAUL and R. JONES

Approved for Public Release

JANUARY 1989

AR-005-570

DEPARTMENT OF DEFENCE
DEFENCE SCIENCE AND TECHNOLOGY ORGANISATION
AERONAUTICAL RESEARCH LABORATORY

AIRCRAFT STRUCTURES REPORT 435

ANALYSIS AND REPAIR OF IMPACT DAMAGED COMPOSITES (U)

by

J. PAUL and R. JONES

SUMMARY

This report discusses the repair of impact damaged graphite/epoxy composite laminates. The behaviour of delamination damage under both uniaxial and biaxial compressive loading is examined and the predictive capabilities of several fracture parameters are investigated. Based upon the results of this analysis a simple repair methodology is proposed and compared with experimental test results.

POSTAL ADDRESS: Director, Aeronautical Research Laboratory,
P.O. Box 4331, Melbourne, Victoria, 3001, Australia

Notation

A	Area.
a	Crack length.
B	Thickness.
C	Compliance.
C_{ijkl}	Stiffness tensor.
C_1	Function of temperature and moisture content.
dV	Change of volume per unit volume.
dV_{max}	Maximum dV.
E_{11}, E_{22}, E_{33}	Elastic modulii of orthotropic lamina.
G	Energy release rate.
J	J-integral.
M	Moisture content.
M_0	Reference moisture content.
n_i	Component of unit normal to integration path in the i-direction.
P	Load.
P_X	Load in X-direction.
P_Y	Load in Y-direction.
T	Temperature.
T_0	Reference temperature.
T^*	T^*-integral.
t_i	Traction component.
u_i	Component of displacement.
V	Volume of material.
W	Strain energy density.
W_{ae}	Strain energy density available to fail the matrix.
W_f	Strain energy density in the fibre.
α_{ij}	Coefficient of thermal expansion.
β_{ij}	Material coefficient related to thermal expansion.
Γ	Integration path enclosing cracktip.
Γ_ϵ	Integration path at a vanishingly small distance from cracktip.
ϵ_{ij}	Strains.
θ_T	Failure angle using T^* approach.
θ_W	Failure angle using energy density approach.
Π	Potential energy.
$\partial\Pi$	Change in potential energy per unit thickness.
σ_{ij}	Component of stress.
ϕ_{ij}	Material coefficient related to moisture expansion.
ψ_{ij}	Coefficient of moisture expansion.

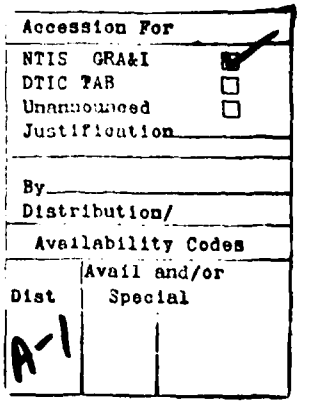

CONTENTS

1. INTRODUCTION

Graphite/epoxy composites have many advantages for use as structural materials in aircraft, including their formability, high specific strength and stiffness, resistance to cracking by fatigue loading and their immunity to corrosion. Apart from producing lighter, more efficient structures, the use of composites should provide more durable structures compared with those manufactured from conventional aluminium alloys. Australian interests in graphite/epoxy composite aircraft structures are focused on the through-life support of the McDonnell-Douglas F/A-18 for the Royal Australian Air Force. A detailed review of damage tolerance from the Australian point of view is given in [1].

Graphite/epoxy composites, while having the above advantages, are prone to a wide range of defects and damage which may significantly reduce residual strength [2-6]. Of the various types of defects, delaminations (i.e. single or multiple internal cracks whose planes are parallel to the surface of a component) [7-9] arising in service are probably the most insidious because they can cause reductions in compressive strength (up to 65% of undamaged strength [10-11]), and are difficult to detect. Delaminations may develop during service due to the presence of excessive interlaminar shear stresses or through-the-thickness tensile stresses at holes, free edges, in the region of section changes and bonded joints. However, the most important source of damage is from impact. Such damage can occur from dropped tools or from stones thrown up from the runway. While impact can cause a significant amount of delamination, often the only external indication is a very slight surface indentation [12,13]. This type of damage is frequently referred to as 'barely visible impact damage' (BVID). The problem of BVID is of particular concern because the damage is unlikely to be discovered unless the region is subjected to non-destructive inspection (NDI). Generally, this employs ultrasonic procedures when BVID is usually readily detectable. However, unfortunately, most routine NDI is likely to be confined to potential hot spots such as critical joints. Frequent full scale NDI is costly and time consuming.

It is highly desirable that procedures are available so that the possible occurrences of delamination-type defects are allowed for in the design and certification of composite aircraft structures and in the development of approaches for through-life support, to provide a rationale for setting inspection intervals, particularly for highly stressed regions and also to provide repair/reject criteria [14,15].

There are two possible methods for repairing this damage. One approach is to remove the damaged region [16-18] and use an internally bonded repair. This is very effective, but requires extensive bonding facilities resulting in a significant period of non-utilization of the component. An alternative approach is to increase the strength by reducing the net sectional stresses. This can be achieved by placing an external patch over the damaged area.

In this report, two fracture criteria, the strain energy density W proposed by Sih [19], and the recent T^*-integral proposed by Atluri [20], are applied to the problem of a composite laminated plate with an impact damaged fastener hole repaired with an externally bonded patch. Tests that were conducted to substantiate the numerical analysis are also described.

2. THE T^* APPROACH

The fracture criteria to be used in this study are T^*-integral proposed by Atluri [20] and the strain energy density approach developed by Sih [19]. The T^*-integral approach will be presented first.

The original formulation of the path-independent J-integral, as presented by Rice [21,22], is given by:

$$J = \int_{\Gamma} (W n_1 - t_i u_{i,1})\, ds \tag{1}$$

where Γ is any closed path surrounding the cracktip, n_1 is the component of the unit normal to the path in the x_1 direction, t_i is the traction vector defined as $t_i = n_j \sigma_{ij}$, u_i is the displacement vector and W is the strain energy density defined as:

$$W = \frac{1}{2}\epsilon_{ij} C_{ijkl} \epsilon_{kl} - \beta_{ij}\epsilon_{ij}(T - T_0) - \sigma_{ij}\epsilon_{ij}(M - M_0) + C_1(T, M) \tag{2}$$

where C_{ijkl} is the stiffness tensor, β_{ij} and σ_{ij} are related to the coefficients of thermal and moisture expansion and C_1 is a fuction of temperature and moisture.

In this analysis we evaluate a modified form of the J-integral, which is defined as T^* [20], and where:

$$T^* = \lim_{\varepsilon \to 0} \int_{\Gamma_\varepsilon} (W n_1 - t_i u_{i,1})\, ds \tag{3}$$

Here the path Γ_ε is a vanishingly small distance from the crack front and in three dimensions must be normal to the crack front. An important characteristic of T^* is that it is evaluated near the crack tip while the traditional J is really a far field parameter. In fatigue crack growth, this distinction becomes significant since reverse plastic deformation can occur upon unloading. Since T^* is evaluated near the tip, it is claimed [20] that it is able to account for the near tip effects while J cannot [23]. In elastic analyses, W is defined as in equation 2 for both T^* and J. However, in the analyses of composite delaminations, it is important to be able to account for local fracture events along a three-dimensional crack front. In elastic analyses, for a through-the-thickness crack propagating under Mode I fracture in a self-similar fashion, J (=T^*) is equivalent to the classical energy release rate G, which is defined as:

$$G = -\frac{\partial \Pi}{\partial A} = -\frac{1}{B}\frac{\partial \Pi}{\partial a} \tag{4}$$

where $\partial\Pi$ is the change in potential energy per unit thickness of the system and ∂a the increment of crack length. When measuring G experimentally, equation 4 is often written as:

$$G = \frac{P^2}{2B}\frac{dc}{da} \tag{5}$$

where P is the applied load, c the compliance as measured by movement of the load points, and B the specimen thickness. However, for three-dimensional delaminations, the growth is usually non self-similar and therefore equation 5 is invalid. Furthermore, equations 4 and 5 are global quantities and do not provide information on near tip events such as

local crack closure. For these cases, measurements of compliances do not yield true values of the crack tip energy release rates, see [24].

Several attempts have been made to expand the definition of energy release rate in equation 4 to include three-dimensional crack growth effects [25-27]. These have resulted in various volume integrals. However, in order to evaluate these formulations using finite element techniques, a prior knowledge of the nature of the crack growth and the shape of the crack front is necessary. Presently, these formulations have been applied successfully only to specimens of simple geometries [28].

The assumption of self-similar crack growth is still inherent in the J^*-integral formulation. Although this assumption is incorrect for three-dimensional analyses of delamination growth, it can be said that for points of maximum crack growth along the crack front, there is sometimes a 'local self-similarity', meaning that locally, the crack front remains parallel. Hence the J^*-integral may be useful in identifying points of maximum crack growth and in estimating the crack initiation load. At points other than the positions of local maximum crack growth, J^* and other similar approaches cannot be said to give the local energy release rate.

Another path dependent and energy related parameter has recently been proposed by Watanabe [29]. This integral, which we will denote as W_f, is given by the first term in the expression for J^* viz:

$$W_f = \lim_{\varepsilon \to 0} \int_{\Gamma_\varepsilon} W n_1 ds \tag{6}$$

3. STRAIN ENERGY DENSITY

In the strain energy density approach failure is assumed to occur when the available energy density W_{av} at a distance r_0 in front of the delamination in the direction of growth reaches a critical value W_c. The value W_c is dependent both on the values of $dV(= \epsilon_{11} + \epsilon_{22} + \epsilon_{33})$ and dA, the change of area per unit area.

For thermomechanical problems

$$W_{av} = \frac{1}{2}\sigma_{ij}\epsilon_{ij} - \frac{1}{2}\sigma_{ij}\alpha_{ij}(T - T_0) - \frac{1}{2}\sigma_{ij}\psi_{ij}(M - M_0) - W_f \tag{7}$$

where α_{ij} and ψ_{ij} are the coefficients of thermal and moisture expansion respectively.

As shown in references [2,31,32] the strain energy density approach has certain advantages over the energy release rate approach. This relationship between this criterion and the other failure criterion was discussed in [24].

For self-similar growth both approaches give residual strengths in good agreement with experimental results [9,31,32]. However, for non-self-similar growth energy release rate concepts must be used with caution.

It should be noted that finite element studies have shown that for delaminations in:

a) composite laminates,
b) at step lap joints, or
c) at mechanically fastened composite joints,

a stage is reached after which a significant increase in the size of the damage does not significantly reduce the residual strength. This significantly simplifies the methodology for estimating critical damage size.

4. THE FINITE ELEMENT MODEL

The problem chosen for this comparative analysis is similar to that used in [32] as a benchmark problem to compare the predictive capabilities of T^* and energy density. However, with the purchase of the F/A-18 by the Royal Australian Airforce (RAAF), attention has been focussed on the use of AS4/3501-6 rather than the T300/5208 graphite/epoxy which was considered in [32]. For this reason the present investigation will use the mechanical properties corresponding to AS4/3601-6.

The problem considered was an impact damaged laminate with a fastener hole loaded under compression. The dimensions of the model are the same as those used in the experimental work of [33]. The structure modelled in this analysis can be seen in Fig. 1 and the finite element mesh for the unrepaired and repaired cases, can be seen in detail in Figs. 2 and 3. The specimen analysed was a $(0/45/0_2/-45/0_2/45/0_2/-45/0)_S$ AS4/ 3501-6 graphite/epoxy laminate and contained a centrally located hole of 9.5 mm diameter, surrounded by delamination damage due to impact and poor drilling.

The elements used were mostly twenty-noded iso-parametric elements with directionally reduced integration and 2 x 2 x 3 Gaussian quadrature points, with the 3 points being taken through the ply thickness. Detailed description of the reduced integration scheme can be found in [34]. The crack tip elements along the circular delamination were fifteen-noded iso-parametric wedge elements. The finite element model contained 2,763 nodes, 528 elements and had 7,611 degrees of freedom. Restraints were applied along the unloaded edges so as to achieve varions levels of restraint representative of a real structure.

The initial damage around the fastener hole was modelled as a circular delamination of radius 13.75 mm between the second and third plies (i.e. between the 45° and 0° plies) [32]. This is an approximate simulation of the initial damage where it was found from ultrasonic C-scanning that the initial delamination was nearly circular [33]. This assumption is further verified in section 9.

The two plies above and below the delamination were modelled separately with ordinary three dimensional elements while the remaining 20 plies were modelled with superelements with displacements varying quadratically in the local iso-parametric co-ordinate system. The material properties used are those of AS4/3501-6 [35] and are tabulated in Table 1.

It is important that, in the finite element model, the faces of the delamination are prevented from overlapping [32]. Otherwise, non-physical solutions may be obtained. By examining the solutions of the displacements, it was found that some parts of the delaminated faces have overlapped. However, unlike earlier work where a system of constraint equations was used, the present work used non-linear gap elements to link all nodes on opposing sides of the delamination surface. Non-linear gap elements set the stiffness of the link to zero unless the two nodes are going to overlap. When this occurs the stiffness of the link is set to a large number thereby stopping the faces from overlapping. This results in an iterative solution process with an increase in computer time, but has the advantage of being fully automated and requiring no initial knowledge of the regions to

local crack closure. A compressive load of 150 kN was applied to the ends of the model in the x-direction (see Fig. 1) and to investigate biaxial effects, a tensile load of either 17 kN or 0 kN was applied in the y-direction.

To investigate the effect of repairing the specimen a 12 ply $(0/+45/0_2/-45/0)_S$ laminate was used as an externally bonded patch covering the damaged area. The patch contained a hole to allow for the possible insertion of a fastener. To evaluate fastener/structure interaction effects the conditions applied to the hole were chose.. to represent:

1) An open hole.
2) An interference fit fastener.
3) A bonded insert.

5. FINITE ELEMENT RESULTS AND DISCUSSION

For each configuration the value of T^* and W_t was computed at each node around the crack tip, as was the local minimum of W_{av}, which in each case corresponded to the local maximum of dV, so as to enable a comparison of the three methods. A summary of the maximum values of T^*, W_{av}, W_t and the corresponding value of dW_{max} is given in Table 2. The angles, at which the respective maxima occur, which are referred to as θ_T and θ_W are also shown.

The variations in the three fracture parameters around the crack front are shown in Tables 3 to 8 (see Fig. 4 for nodal positions), which give the values of T^*,W_{av} and W_t at selected points. The variation in W_{av} is similar to that of T^*. The two plies above the delamination move out of plane, i.e. crack opening and/or closure. For all of the cases analysed this out of plane movement was non-symmetric (see Figs. 5 and 6). This asymmetry results in the asymmetric growth of the delamination which is consistent with C-scan and thermal emmission measurements, see [36].

The results of this analysis suggest that:

(1) Load biaxiality has a marked effect on the fracture parameters and hence on the failure of structural components. The fracture parameter T^* is less affected by load biaxiality than is W_{av} and W_t.

(2) For all cases considered the location of the maximum values of both parameters were similar.

(3) When the patch material has the same stiffness as the parent laminate the reductions in T^*, W_{av} and W_t can be estimated by multiplying the values corresponding to the unrepaired structure with the square of the reduction in the net sectional stress. This infers that the residual strength of a repaired structural component can be estimated by the following simple formulae:

$$\frac{\text{Residual Strength (repaired)}}{\text{Residual Strength (unrepaired)}} = \sqrt{\frac{W(\text{unrepaired})}{W(\text{repaired})}} \tag{7}$$

where W is the energy density in the laminate in the region of the patch. Whilst this formulae can account for multiaxial loading, in the case for a uniaxial load it reduces, when the patch has the same effective moduli as the parent laminate, to

$$\frac{\textit{Residual Strength (repaired)}}{\text{Residual Strength (unrepaired)}} = \frac{\sigma(\textit{unrepaired})}{\sigma(\text{repaired})} \tag{8}$$

The energy density in both the repaired and the unrepaired structure can be computed from a knowledge of strain gauge results before and after repair.

(4) Prohibiting local bending at the hole had an insignificant effect on the fracture parameters. However, prohibiting in-plane movement and local bending reduced T^* whilst not reducing W_{ar} and increasing W_f. This reduction in T^* would correspond to an increase in the failure load of between 11 to 16%.

Unlike T^*, W_{ar} was essentially unaffected by this restraint. As a result, experimental results are required to evaluate this effect further.

(5) Energy density theory predicted that for most cases damage growth would be predominantly in-plane.

6. COMPRESSION TESTS

The experimental work focused on the use of an externally bonded repair to reduce the net sectional stresses. Static compressive tests were conducted on composite specimens to show that provided the global bending is restrained, the increase in the residual strength can be estimated by the following simple formula:-

$$\frac{\text{Residual Strength (repaired)}}{\text{Residual Strength (unrepaired)}} \approx \frac{\sigma(\text{unrepaired})}{\sigma(\text{repaired})} \tag{7}$$

Two series of tests were carried out. The preliminary tests were aimed at developing a test methodology to provide an acceptable level of global restraint. The material used in these tests was considered to be unacceptable, because of its inability to provide valid C-scan results, thereby rendering the results unacceptable. The methodology developed was then used to obtain failure load/strain data for unrepaired and repaired test specimens.

Three impact damage sizes were chosen. In each case the damage was anticipated to lie on the flat or near the flat part of the residual strength versus damage area curve (see Fig. 7) [37].

7. SPECIMEN FABRICATION

The graphite epoxy material used throughout these tests was AS4/3501-6. The parent material was laid up in sheets of 300mm x 900mm, with a ply configuration of $[(+45_2/-45_2/0_4)_3/90]_S$.

Before the specimens were cut from these panels, the panels were C-scanned to determine the void content of the material. Two different sizes of specimens were cut. The smaller specimens were used to develop the test methodology, whilst the larger specimens were used for the main series of tests (see Fig. 8). The working gauge lengths of the two sizes of specimens were 120mm and 250mm respectively.

Each specimen was impacted with a 1/2" diameter ball bearing with a mass of 1 kg and from a height of 1.3m. The impact test rig can be seen in Fig. 9. The specimens were placed between two thick steel plates; with holes

drilled to the size of damage required. The absorbed energy was calculated by differencing the initial kinetic energy and the rebound kinetic energy. A laser located on the bottom right hand side of the rig (see Fig. 9) was triggered when the impactor cut the beam. The initial and rebound pulses were recorded on a digital oscilloscope (NICOLET 2090 MODEL 207). The data was then analysed by a HP 9816 computer and a typical plot of time versus distance is shown in Fig. 10.

For the specimens used in the preliminary set of tests, the hole diameter of the steel restraint plates used in the impact test rig, was 30mm. For the main test series a range of hole diameters used were namely 20mm, 30mm and 40mm. A summary of the absorbed energies can be found in Table 9. This Table also outlines which specimens were repaired, or left unrepaired and the average damage area created by the impactor.

Each specimen contained a 6mm diameter centrally located hole, simulating a fastener hole, as was previously analysed. The hole was drilled using a diamond-tipped core drill and was cooled by water, restrained by a plasticine dam.

All specimens were subjected to a C-scan of the impacted area. The damage size can be approximated from the C-scan results; a typical C-scan is shown in Fig. 11.

8. REPAIR FABRICATION

In order to validate the simple design rule previously postulated it was required that the effective stiffness and ply configuration of the patch be representative of the parent material. The material used for the patch was AS4/3501-6 and was 16 plies thick, with a ply configuration of $[0_2/\pm 45/\mp 45/0_2]_S$. The ends of the patch were scarfed as shown in Fig. 12. The length of the patches and distance to edge of the grips, for the two series of tests were 80mm, 40mm and 190mm, 60mm respectively.

The patches were bonded to the parent laminate using the cold setting acrylic adhesive FLEXON 241. The adhesive was chosen for its shear strength, ease of application and because environmental effects were not an issue in this test series.

9. TEST METHODOLOGY

Data from the tests were acquired in two ways. For the preliminary tests, displacement transducers were bonded onto the specimens and a plot of load versus displacement was obtained. For the main series of tests, it was decided that far field strain gauges would produce more useful data. The gauges show the average far field failure strains and also indicate the extent of bending in the specimens.

Four strain gauges were bonded to each of the unrepaired specimens as shown in Fig. 13, whilst each repaired specimen had two strain gauges located on the patched side as also shown in Fig. 13. In each case the gauges were 110mm from the edge of the hole. This meant that both the repaired and unrepaired specimens had gauges located in the same position relative to the hole.

An HP 9816 computer program was written to acquire the strain readings at a rate of approximately 3 to 5 Hz. The program allowed the technician to scan the strain gauges at particular load increments or continuously. After the test, the data was stored on a floppy disk such that it could be analysed by the laboratory's main data acquisition program [38].

In order to achieve the required level of restraint in the specimen, an anti-buckling rig had to be used. Preliminary tests involved the modification of this rig until the final format was reached (see Figs. 14 and 15). The edges of the specimen were restrained by four bars, with a further four cross bars connected to these bars and the anti-buckling rig, in order to provide the required bending restraint.

In the process of developing the test rig it was noted that, when testing the repaired specimens, severe bending occured due to the shift in the neutral axis due to the patch. To alleviate this problem, all patched specimens were tested back to back. The specimens were separated by an aluminium spacer with a cut out region, i.e. a window, the size of the working area of the specimen and with a 5mm strip down each side (see Fig. 16). A window was used so that local bending of the delamination area was free to occur (see section 4). It was thought that restraining the delamination from opening would result in an unrealistic stiffness reading. Two repaired specimens were then bonded to either side of the spacer with an Araldite epoxy . This was thought to aid in the load transfer process from the grips to the specimens. This test configuration prevented global bending of the specimens whilst permitting local bending of the delaminated region.

All experiments were conducted in a 500 kN dynamic and 625 kN static Testing Machine. The loading rate for each specimen was 20 kN/min. The loads and strains were recorded continuously in the preliminary tests using an x-y plotter. In the main series of tests recording of the data was done at load increments of 10 kN. Continuous scanning was activated at 170 kN for the unrepaired specimens and at 400 kN for the repaired specimens. All specimens were tested to failure.

10. TEST RESULTS AND DISCUSSION

The preliminary tests provided valuable information on various aspects of composite compressive testing. The most noticeable problem was the global bending of the specimens in the test rig. After several modifications to the anti-buckling rig global bending was minimized, resulting in tests representative of a structural component which is essentially restrained against out-of-plane bending. Minimal global bending of damaged components will always occur, due to the non-symmetric nature of impact damage in composites. Furthermore, for specimens with nominally the same damage area, or absorbed energy, the level of intraply cracking is unlikely to be identical.

Quality control in the manufacture of composite material is another problem which was encountered. Several of the panels received had significant thickness variations resulting in resin rich areas and resin void areas. Large variations in absorbed energies were seen when impacting specimens manufactured from this material. However, even though the 'bad' material did not produce valid C-scan results, the average failure strains were 4% higher than the 'good' material.

In the main series of tests, all specimens, except two which exhibited extensive bending*, produced load versus strain curves which were essentially linear to failure. The failure strains for each specimen can be found in Table 9. The failure strains follow the asymptotic nature outlined in [37,40] and a plot of residual strength versus damage area can be found in Fig. 17. For a given damage size the different forms of internal damage, due to impact, were reflected in a slight variation in the failure strains. The experiments were conducted with the testing machine in load control. There was a time delay before the machine released the load. This resulted in extensive damage occuring to the specimens (see Figs. 18 and 19). The patches and adhesive bond failed after the failure of the parent laminate.

The failure load of the repaired specimen can be predicted (see Table 9) using equation 7 and requires only a knowledge of the unrepaired residual strength and the change in net sectional stresses due to patching. The change in net sectional stress can be readily calculated from the change in net sectional area. This result is believed to substantiate the trends predicted in the previous chapter and significantly simplifies the repair design philosophy.

It was shown in [40] that, a stress reduction of 10% can produce a 100 fold change in life. This reduction in stress can easily be obtained using an external patch. The use of an external patch method avoids the requirement for complete removal of the damage area, resulting in speedier and simpler repairs for in-service structural components.

11. CONCLUSIONS

This paper has presented a repair methodology that can be used as a quick first approximation to field repairs of impacted damaged composite structures. The use of externally bonded patches has the advantage of being easily and quickly applicable. In certain cases, the existing internal delamination damage does not have to be removed.

The analyses revealed, after close examination of the stresses and change in volume around the crack front, that the dominant mode of failure was Mode II. As seen in [40], Mode I tests provide more consistent values of energy release rate than those obtained from Mode II tests. This infers that additional research is required to fully understand the implications of delamination failure by Mode II.

The present analysis has revealed that load biaxiality has a marked effect on the linear-elastic fracture parameters. This infers a corresponding effect on residual strength. Given the absence of experimental data an experimental program to verify this prediction is necessary. It is also conjectured that when using an externally bonded repair on thick supported structures, the increase in the residual strength is proportional to the reduction in the net sectional stress provided that the repair is of similar effective stiffness.

* The patched specimens 4 and 5 had vastly different absorbed energies and the patches were not exactly in line, thereby inducing extensive bending near and up to failure.

REFERENCES

1. Baker A.A., Jones R. and Callinan R.J., 'Damage Tolerance of Graphite/Epoxy Composites', Composite Structures Vol. 4, No. 1, pp15-44 (1985).
2. Badaliance R. and Dill H.D., 'Damage Mechanism and Life Prediction of Graphite-Epoxy Composites', Damage in Composite Materials, ASTM STP 775, pp229-242, (1982).
3. Schutz D., Gerharz J.J. and Alschweig E., 'Fatigue Properties of Unnotched, Notched and Jointed Specimens of a Graphite-Epoxy Composite', Fatigue of Fibrous Composite Materials, ASTM STP 723, pp31-47, (1981).
4. Prakash R., 'Significance of Defects in the Fatigue Failure of Carbon Fibre Reinforced Plastics', Fibre Science and Technology Vol. 14, pp171-181, (1981).
5. Talreja R., 'A Conceptual Framework for the interpretation of Fatigue Damage Mechanisms in Composite Materials", J. Composites Technology and Research Vol. 7, pp25-29, (1985).
6. Harris B., 'Fatigue and Accumulation of Damage in Reinforced Plastics', Composites Vol. 8, pp214-220, October (1977).
7. Ramkumar R.L., 'Compression Fatigue Behaviour of Composites in the Presence of Delaminations', *Damage in Composite Materials*, ASTM STP 775, pp184-210, (1982).
8. O'Brien T.K., 'Mixed-Mode Strain-Energy-Release Rate Effects on Edge Delamination of Composites', Effects of Defects in Composite Materials, ASTM STP 836, pp125-142, (1984).
9. Jones R., Broughton W., Mousley R.F. and Potter R.T., 'Compression Failures of Damaged Graphite Epoxy Laminates', Composite Structures Vol. 3, pp167-186, (1985).
10. Ramkumar R.L., 'Effect of Low-Velocity Impact Damage on the Fatigue Behaviour of Graphite-Epoxy Laminates', Long-Term Behaviour of Composites, ASTM STP 813, pp116-135, (1983).
11. Rosenfeld M.S. and Gause L.W., 'Compression Fatigue Behaviour of Graphite-Epoxy in the Presence of Stress Raisers', Fatigue of Fibrous Composite Materials, ASTM STP 723, pp174-196, (1981).
12. Adsit N.R. and Waszczak J.P. 'Effect of Near-Visual Damage on the Properties of Graphite/Epoxy', Composite Materials: Testing and Design (Fifth Conference) ASTM STP 674, pp101-117, (1979).
13. Starnes J.H.Jr., Rhodes M.D. and Williams J.G., 'Effect of Impact Damage and Holes on the Compressive Strength of a Graphite/Epoxy Laminate', Nondestructive Evaluation and Flaw Criticality for Composite Materials, ASTM STP 696, pp145-171, (1979).

14. Williams J.G., O'Brien T.K. and Chapman A.J. III., 'Comparison of Toughened Composite Laminates using NASA Standard Damage Tolerance Tests', ACEE Conf. on Composite Structures Technology, Seattle, Washington, 3th-15th August (1984).

15. Carden H.D., 'Impact Dynamics Research on Composite Transport Structures", ACEE Conf. on Composite Structures Technology, Seattle, Washington, 3th 15th August (1984).

16. Hart-Smith L.J., 'The Design of Repairable Advanced Composite Structures', Douglas Paper 7550, Presented to SAE Aerospace Technology Conference, Long Beach, California, 14th - 17th October (1985).

17. Kurachi E.A. and Hart-Smith L.J., 'Design Details for Adhesively Bonded Repairs of Fibrous Composite Structures', Douglas Paper 7637, Presented to 31st National Sample Symposium and Exhibition, Las Vegas, 8th-10th April (1986).

18. Hart-Smith L.J., 'Design and Analysis of Bonded Repairs for Metal Aircraft Structures', Bonded Repair of Aircraft Structures, ed. Baker A.A. and Jones R., Martinus Nijhoff Publishers, pp31-46, (1988).

19. Sih G.C., Mechanics of Fracture 6: Cracks in Composite Materials, Martinus Nijhoff Publishers, The Hague, XVI-LX-XXI, (1981).

20. Brust F.W., McGowan J.J. and Atluri S.N., 'A Combined Numerical/Experimental Study of Ductile Crack Growth after a Large Unloading, using T^*, J and CTOA criteria, Engng. Frac. Mech. Vol. 23, No. 3, pp537-550, (1986)

21. Rice J.R., 'Mathematical Analysis in the Mechanics of Fracture', in Fracture - An Advanced Treatise, Vol. 2, Mathematical Fundamentals, Ed. Liebowitz H., Academic Press, (1968).

22. Rice J.R., 'A Path Independent Integral and the Approximate Analysis of Strain Concentration by Notches and Cracks', J. Appl. Mech. Vol. 90, pp379-387, June (1968).

23. Agarwal B.D., Prashant K. and Patro B.S., 'The J-integral as a Fracture Criterion for Composite Materials', Composite Structures 2, Ed. I.H. Marshall, Applied Science Publishers, London, (1983).

24. Molent L., Paul J. and Jones R., 'Criteria for Matrix Dominated Failure', Aircraft Structures Report 432, Aeronautical Research Laboratory, February, (1988).

25. de Lorenzi H.G., 'On the Energy Release Rate and the J-Integral for 3-D Crack Configurations", Int. J. Frac. Vol. 19, pp183-193, (1982).

26. de Lorenzi H.G., 'Energy Release Rate Calculations by the Finite Element Method', Engng. Frac. Mech. Vol. 21 No. 1, pp129-143, (1985).

27. Li F.Z., Shih C.F. and Needleman A., 'A Comparison of Methods for Calculating Energy Release Rates", Engng. Frac. Mech. Vol. 21, No. 2, pp405-421, (1985).

28. Dodds Jr. R.H., Carpenter W.C. and Sorem W.A., 'Numerical Evaluation of a 3-D *J*-integral and Comparison with Experimental Results for a 3-Point Bend Specimen', Engng. Frac. Mech. Vol. 29, No. 3, pp275-285, (1988).

29. Watanabe, K. and Sato, Y., 'Some Considerations on Inelastic Crack Parameters and Path-Independent Integrals', Proc. Intern. Conf. on Fracture and Fracture Mechanics, Shanghai, 1987, edit. by C. Ouyang et. al., Fudan University Press, China, (1987).

30. Kantorovich L.V. and Krylov V.I., 'Approximate Methods of Higher Analysis', P. Noordhoff Ltd., (1958).

31. Chou S.C., 'Delamination of T300/5208 Graphite/epoxy Laminates' , Proceedings 2nd USA-USSR Conference on Fracture of Composites , edited by G.C. Sih and V.P. Tazmus, Martinus Nijhoff Press , Netherlands, pp 247-264, (1982).

32. Tay, T.E., Williams, J.F. and Jones, R., 'Application of the T^* Integral and S criteria in Finite Element Analysis of Impact Damaged Fastener Holes in Graphite/epoxy Laminates Under Compression', Composite Structures, Vol. 7, No. 4, pp233-253, (1987).

33. Adsit N.R. and Waszczak J.P. 'Effect of Near-Visual Damage on the Properties of Graphite/Epoxy', Composite Materials: Testing and Design (Fifth Conference) ASTM STP 674, pp101-117, (1979).

34. Jones R., Callinan R., Teh K.K. and Brown K.C., 'Analysis of Multilayer Laminates using Three-Dimensional Super Elements', Int. J. Numer. Methods Engng. Vol. 18, pp583-587, (1984).

35. Murray J.E. and Birchfield E.B., 'Material Substantiating Data and Analaysis Report', McDonnell Aircraft Company, Report Number MDC A5253, August (1978).

36. Ryder J.D., Lauraitis K.N. and Pettit D.E., 'Advanced Residual Strength Degradation Rate Modelling for Advanced Composite Structures', AFWAL-TR-79-3095, Vol. II - Tasks II and III, July (1981).

37. Bishop S.M., Dorey G., 'The Effect of Damage on the Tensile and Compressive Laminate', AGARD CP No. 355, 12th - 14th April 1983 pp10.1-10.10.

38. Paul J.J. 'Data Logger Application Program Manuel', Aeronautical Research Laboratory Internal Report, D.S.T.O., Melbourne, Australia, February (1985).

39. Dorey G., Sigety P., Stellbrink K., 't Hart W.G.J. 'Impact Damage Tolerance of a Carbon Fibre Composite Laminate', Technical Report 84049 GARTEUR/TP-007, May (1984).

40. Jones, R., Paul, J.J., Tay, T.E. and Williams, J.F., 'Assessment of the Effect of Impact Damage in Composites: Some Problems and Answers', Theoretical and Applied Fracture Mechanics, Vol. 9, pp83-95, (1988)

Table 1: MECHANICAL PROPERTIES OF AS4/3501-6.

E_{11} (MPa)	E_{22} (MPa)	E_{33} (MPa)	μ_{12}	G_{12} (MPa)	G_{13} (MPa)	G_{23} (MPa)
128,200	13,800	13,800	0.3	5,857	5,857	5,857

Table 2: SUMMARY OF T^*, W_{av}, dW_{max} AND W_t

Case	T^*	θ_T	Predicted T^*	dW_{max}	W_{av}	θ_W	Predicted W_{av}	W_t	Predicted W_t
1UN	0.0907	30°	—	-0.00126	0.5176	30°	—	0.0503	—
2UN	0.0901	30°	—	-0.00125	0.5175	30°	—	0.0508	—
3UN	0.0687	45°	—	-0.00118	0.5194	30°	—	0.0648	—
1UR	0.0471	45°	0.0403	-0.00121	0.2672	30°	0.2300	0.0272	0.0224
2UR	0.0470	45°	0.0400	-0.00119	0.2673	30°	0.2300	0.0274	0.0226
3UR	0.0376	45°	0.0305	-0.00113	0.2693	30°	0.2308	0.0283	0.0288
1BN	0.1390	30°	—	0.00448	1.0753	30°	—	0.1160	—
2BN	0.1390	30°	—	0.00447	1.0732	30°	—	0.1150	—
3BN	0.0992	30°	—	0.00358	1.0728	30°	—	0.1720	—
1BR	0.0669	30°	0.0618	0.00290	0.4968	30°	0.4779	0.0561	0.0516
2BR	0.0669	30°	0.0618	0.00176	0.4968	30°	0.4779	0.0551	0.0511
3BR	0.0514	30°	0.0441	0.00236	0.5025	30°	0.4768	0.0790	0.0764

Case Description: 1 — Open hole, 2 — Interference Fit Fastener, 3 — Bonded Insert

U — Uniaxial Load, B — Biaxial Load, N — No Repair, R — Repaired.

Table 3: UNIAXIAL T^* RESULTS AROUND THE CRACK FRONT.

Unrepaired			
Node Number	Open Hole	Interference Fit Fastener	Bonded Insert
36	0.0889	0.0887	0.0687
526	0.0907	0.0901	0.0666
528	0.0085	0.0065	0.0310
49	0.0358	0.0355	0.0161
531	0.0007	0.0013	0.0043
533	0.0270	0.0264	0.0215
45	0.0334	0.0328	0.0258

Repaired (Patch (O,+45,O2,-45,O)s)			
Node Number	Open Hole	Interference Fit Fastener	Bonded Insert
36	0.0471	0.0470	0.0376
526	0.0467	0.0464	0.0366
528	0.0076	0.0648	0.0179
49	0.0124	0.0123	0.0051
531	0.0004	0.0439	0.0073
533	0.0157	0.0154	0.0122
45	0.0170	0.0169	0.0134

Table 4: BIAXIAL RESULTS T^* RESULTS AROUND THE CRACK FRONT.

Unrepaired			
Node Number	Open Hole	Interference Fit Fastener	Bonded Insert
36	0.1090	0.1080	0.0918
526	0.1390	0.1390	0.0992
528	0.0149	0.0178	0.0378
49	0.0502	0.0499	0.0051
531	0.0351	0.0351	0.0372
533	0.0587	0.0582	0.0330
45	0.0683	0.0626	0.0527

Repaired (Patch (O,+45,O2,-45,O)s)			
Node Number	Open Hole	Interference Fit Fastener	Bonded Insert
36	0.0554	0.0553	0.0470
526	0.0669	0.0669	0.0514
528	0.0077	0.0095	0.0187
49	0.0208	0.0208	0.0025
531	0.0147	0.0147	0.0163
533	0.0271	0.0267	0.0189
45	0.0279	0.0278	0.0252

Table 5: UNIAXIAL W_{av} RESULTS AROUND THE CRACK FRONT.

Unrepaired			
Node Number	Open Hole	Interference Fit Fastener	Bonded Insert
196	0.5061	0.5065	0.4017
660	0.5176	0.5175	0.5194
662	0.3042	0.3036	0.2969
666	0.0967	0.0974	0.0981
668	0.1264	0.1257	0.1260
670	0.4879	0.4873	0.4944
664	0.5163	0.5160	0.5196

Repaired (Patch (O,+45,O2, -45,O)s)			
Node Number	Open Hole	Interference Fit Fastener	Bonded Insert
196	0.2594	0.2597	0.2655
660	0.2672	0.2673	0.2693
662	0.1595	0.1592	0.1607
664	0.0497	0.0501	0.0558
666	0.0659	0.0656	0.1089
668	0.2453	0.2451	0.2474
670	0.2596	0.2595	0.2592

Table 6: BIAXIAL RESULTS W_{av} RESULTS AROUND THE CRACK FRONT.

Unrepaired			
Node Number	Open Hole	Interference Fit Fastener	Bonded Insert
196	0.8848	0.8845	0.9318
660	1.0753	1.0732	1.0728
662	0.8333	0.8306	0.7870
664	0.4639	0.4638	0.4371
666	0.7590	0.7572	0.7584
668	1.0540	1.0520	1.0748
670	0.8968	0.8964	0.9211

Repaired (Patch (O,+45,O2,-45,O)s)			
Node Number	Open Hole	Interference Fit Fastener	Bonded Insert
196	0.4074	0.4076	0.4267
660	0.4968	0.4968	0.5025
662	0.3766	0.3753	0.3676
664	0.2001	0.1998	0.1971
666	0.3604	0.3590	0.3583
668	0.4992	0.4988	0.5029
670	0.4192	0.4193	0.4238

Table 7: UNIAXIAL W_i RESULTS AROUND THE CRACK FRONT.

Unrepaired			
Node Number	Open Hole	Interference Fit Fastener	Bonded Insert
36	0.0503	0.0508	0.0551
526	0.0421	0.0432	0.0648
528	0.0424	0.0418	0.0322
49	0.0472	0.0053	0.0079
531	0.0112	0.0115	0.0204
533	0.0339	0.0334	0.0319
45	0.0484	0.0483	0.0503

Repaired (Patch (O,+45,O2,-45,O)s)			
Node Number	Open Hole	Interference Fit Fastener	Bonded Insert
36	0.0272	0.0274	0.0267
526	0.0209	0.0215	0.0283
528	0.0212	0.0209	0.0170
49	0.0020	0.0022	0.0041
531	0.0059	0.0062	0.0112
533	0.0189	0.0186	0.0169
45	0.0263	0.0262	0.0268

Table 8: BIAXIAL RESULTS W_i RESULTS AROUND THE CRACK FRONT.

Unrepaired			
Node Number	Open Hole	Interference Fit Fastener	Bonded Insert
36	0.0496	0.0496	0.1010
526	0.0467	0.0476	0.1720
528	0.1160	0.1150	0.0431
49	0.0644	0.0639	0.0518
531	0.0056	0.0066	0.0142
533	0.0626	0.0621	0.0484
45	0.0749	0.0746	0.0574

Repaired (Patch (O,+45,O2,-45,O)s)			
Node Number	Open Hole	Interference Fit Fastener	Bonded Insert
36	0.0267	0.0267	0.0476
526	0.0231	0.0235	0.0790
528	0.0562	0.0555	0.0241
49	0.0290	0.0285	0.0252
531	0.0013	0.0011	0.0090
533	0.0321	0.0318	0.0247
45	0.0375	0.0373	0.0298

Table 9: RESULTS OF STATIC COMPRESSION TESTS.

Specimen Number	Impactor Diameter	Absorbed Energy	Damaged Area	Unrepaired (U) Repaired (R)	Failure Load	Failure Strain	Predicted Strain
	(mm)	(J)	(mm^2)		(kN)	($\mu\epsilon$)	($\mu\epsilon$)
1	19.8	7.59	453	U	-190.9	-4503	-
2	19.8	7.55	453	U	-213.6	-4680	-
3	19.8	7.96	453	U	-213.1	-4826	-
4	19.8	5.60	479	R	-238.1	-4993*	-6164
5	19.8	8.21	428	R	-238.1	-4993*	-6164
6	19.8	7.84	448	R	-289.3	-6699	-6164
7	19.8	7.88	458	R	-289.3	-6699	-6164
8	30.0	7.46	733	U	-168.0	-4097	-
9	30.0	6.93	718	U	-191.5	-4375	-
10	30.0	7.88	665	U	-173.2	-4305	-
11	30.0	7.54	761	U	-195.6	-4350	-
12	30.0	7.74	761	U	-197	-4274	-
13	30.0	7.67	761	U	-178.0	-4025	-
14	30.0	7.66	800	R	-233.2	-5293	-5594
15	30.0	7.35	800	R	-233.2	-5293	-5594
16	30.0	7.45	739	R	-227.0	-5554	-5594
17	30.0	7.64	704	R	-227.0	-5554	-5594
18	39.7	6.25	1252	U	-178.5	-4061	-
19	39.7	5.76	1252	U	-204.0	-4445	-
20	39.7	5.87	1252	U	-180.9	-4090	-
21	39.7	7.83	1385	R	-237.6	-5337	-5542
22	39.7	7.58	1212	R	-237.6	-5337	-5542
23	39.7	7.70	1290	R	-222.4	-5099	-5542
24	39.7	7.59	1120	R	-222.4	-5099	-5542

* Specimens exhibited extensive bending prior to failure (anti-buckling rig was distorted)

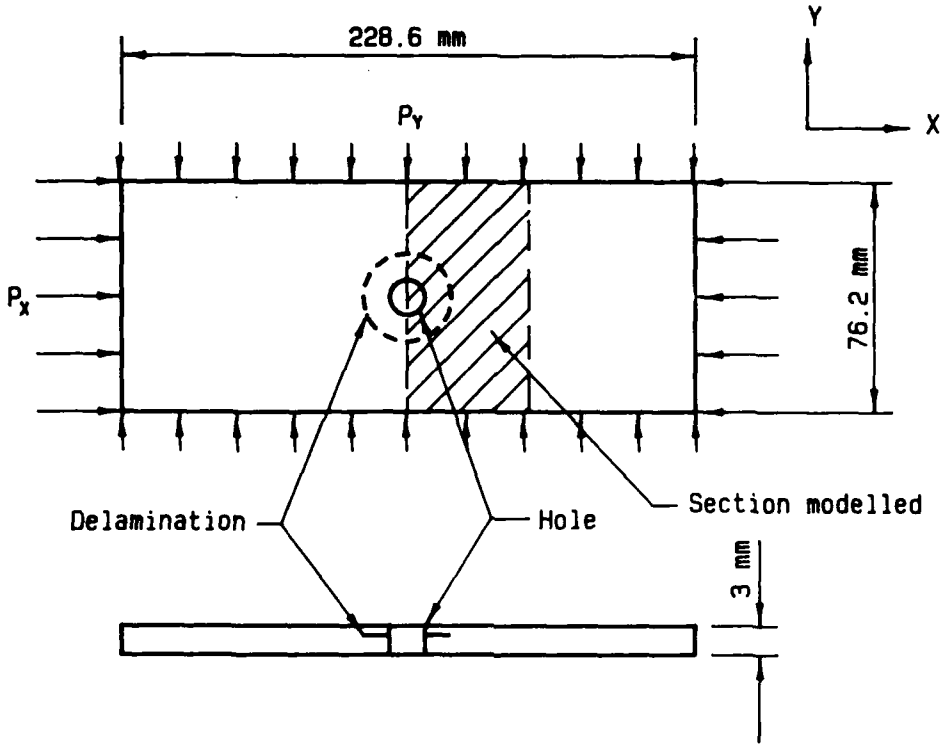

FIG 1: DAMAGED HOLE STRUCTURE.

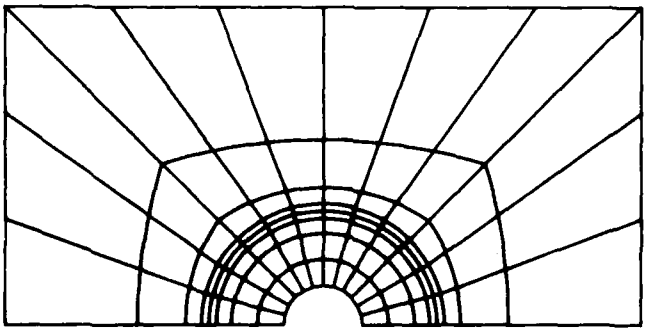

FIG 2a): PLAN VIEW OF THE FINITE ELEMENT MESH.

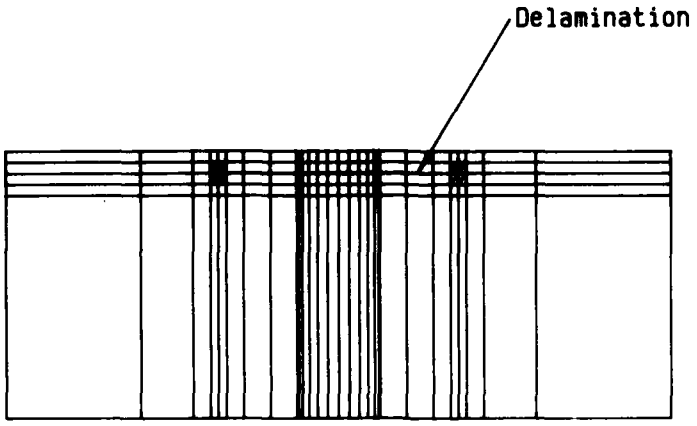

FIG 2b): CROSS-SECTIONAL VIEW OF THE UNREPAIRED FINITE ELEMENT MESH.

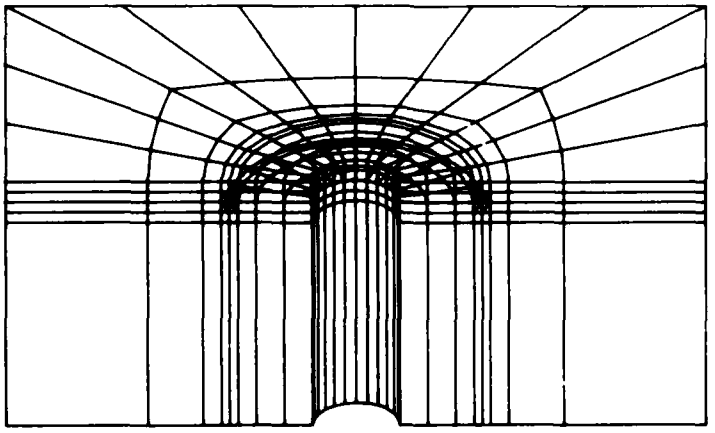

FIG 2c): PERSPECTIVE VIEW OF THE UNREPAIRED FINITE ELEMENT MESH.

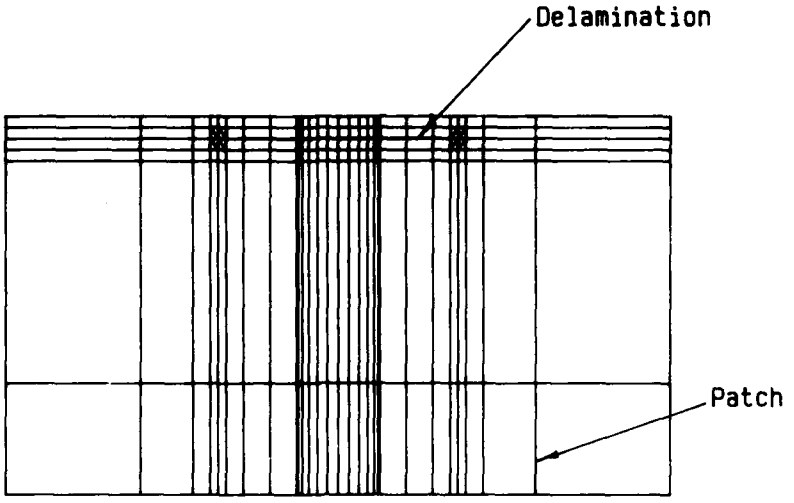

FIG 3a): CROSS-SECTIONAL VIEW OF THE REPAIRED FINITE ELEMENT MESH.

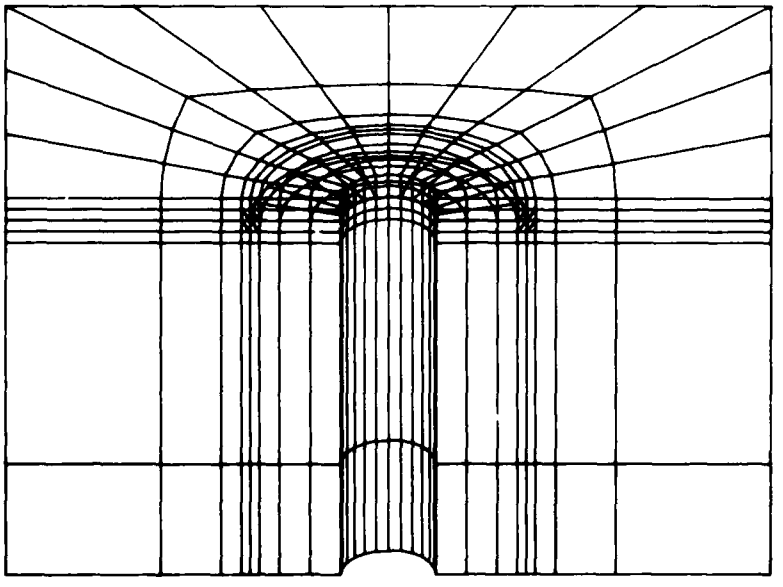

FIG 3b): PERSPECTIVE VIEW OF THE REPAIRED FINITE ELEMENT MESH.

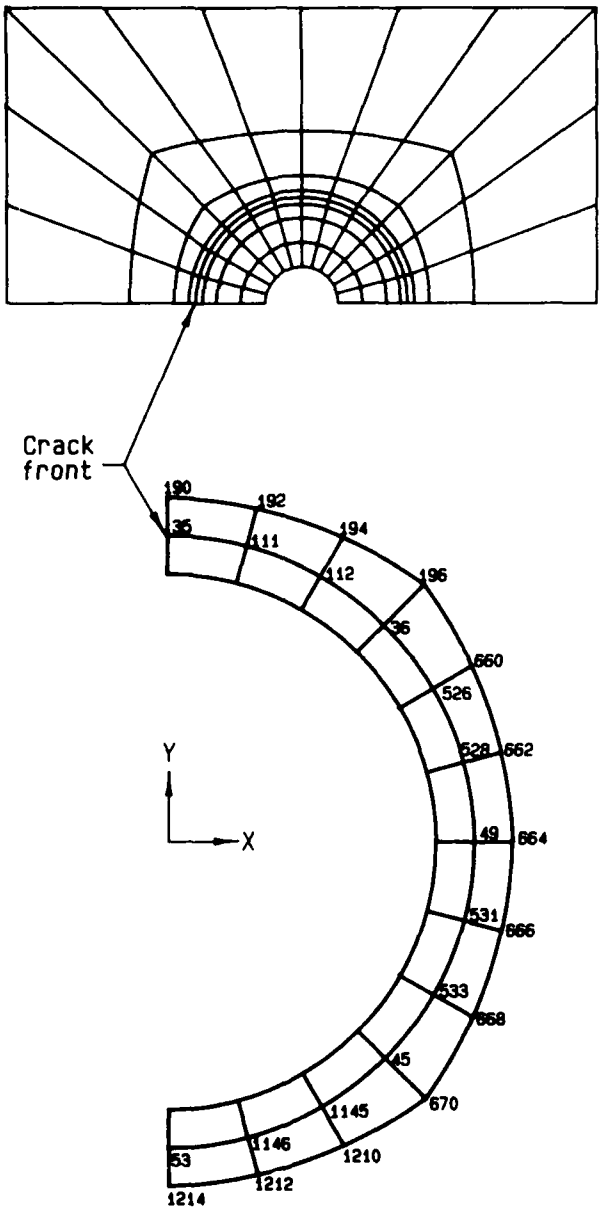

FIG 4: NODAL POSITIONS AROUND CRACK FRONT.

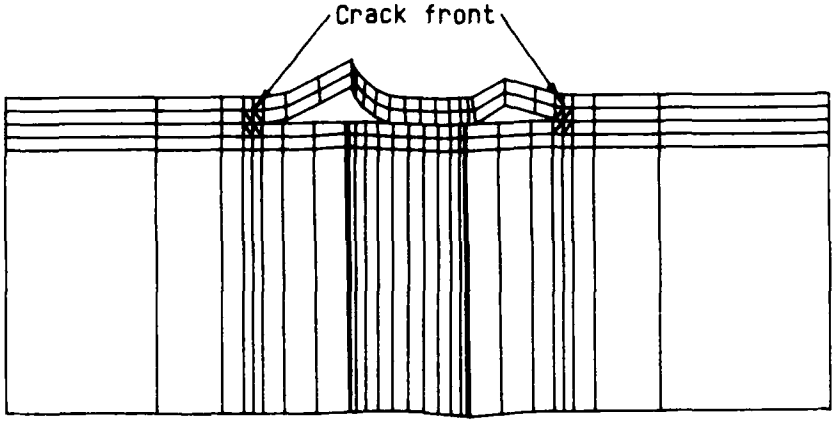

FIG 5a): UNREPAIRED STRUCTURAL DEFORMATIONS, SIDE VIEW.

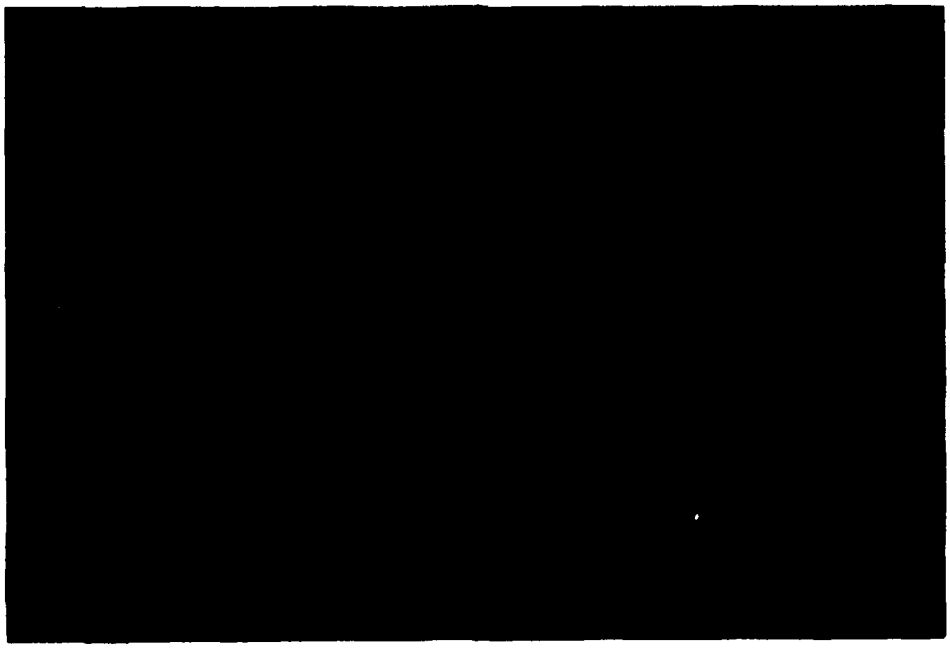

FIG 5b): UNREPAIRED STRUCTURAL DEFORMATIONS, PERSPECTIVE VIEW.

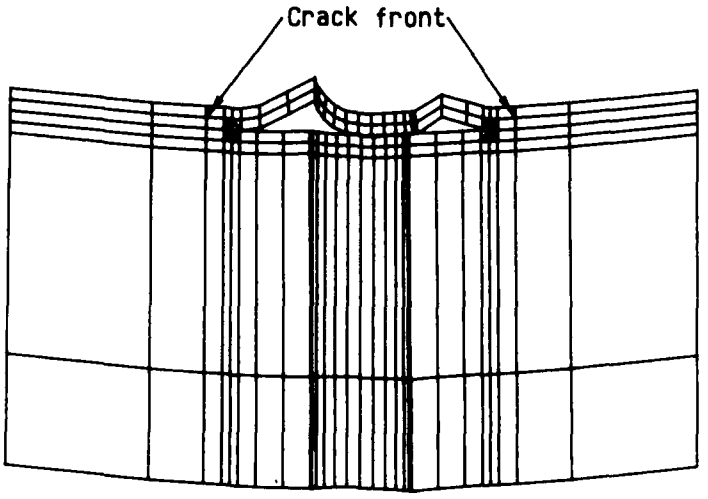

FIG 6a): REPAIRED STRUCTURAL DEFORMATIONS, SIDE VIEW.

FIG 6b): REPAIRED STRUCTURAL DEFORMATIONS, PERSPECTIVE VIEW.

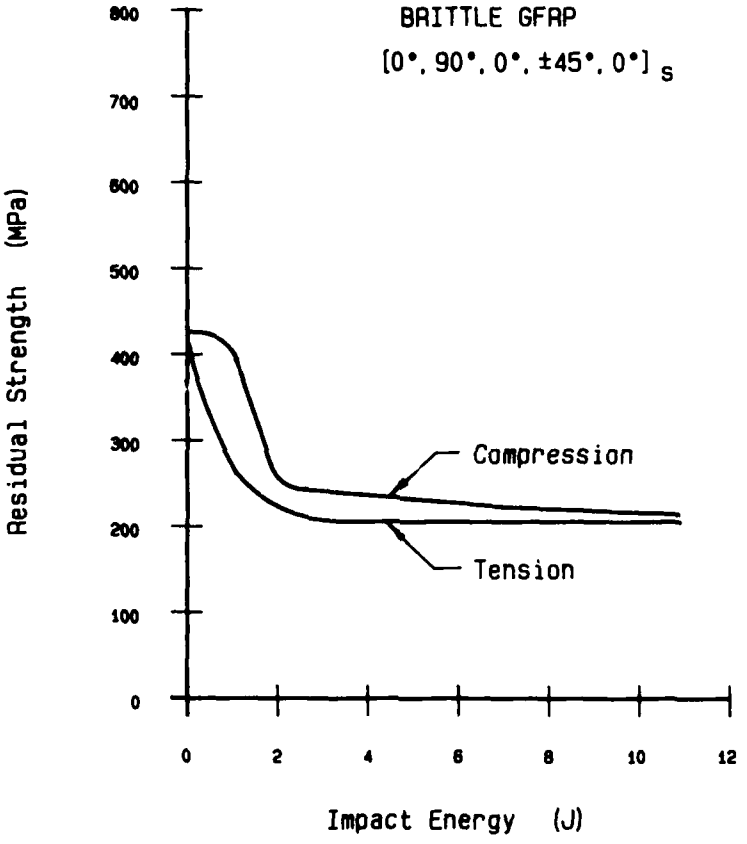

FIG 7: TYPICAL RESIDUAL STRENGTH VERSUS IMPACT ENERGY CURVE OF GFRP, FROM [37].

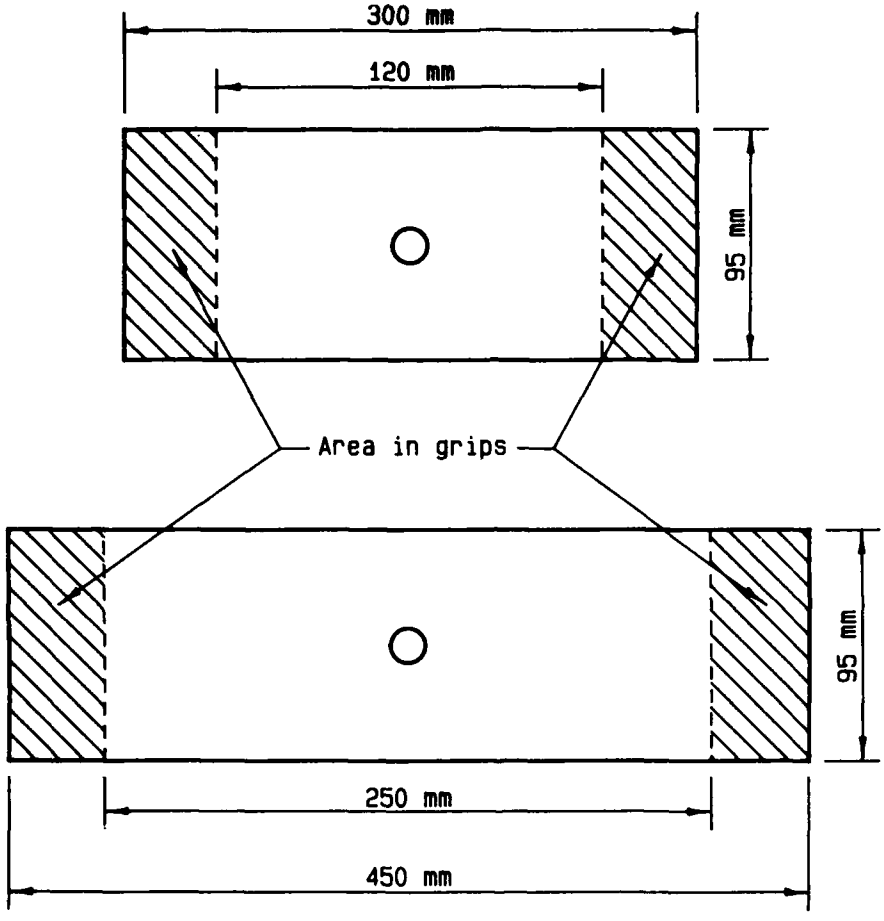

FIG 8: EXPERIMENTAL TEST SPECIMENS, SMALL AND LARGE COUPONS.

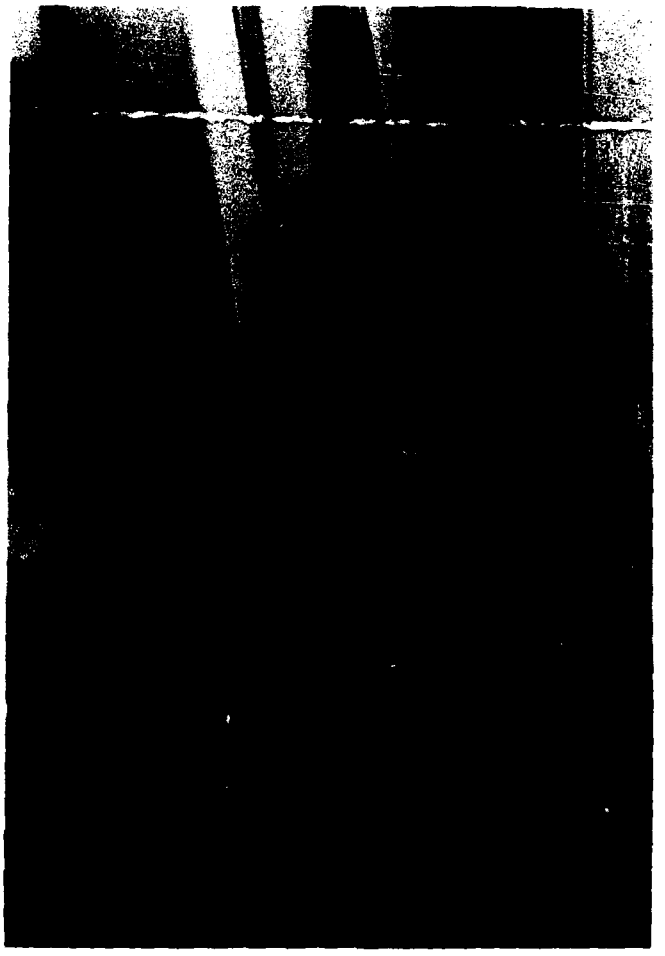

FIG 9: IMPACT TEST RIG.

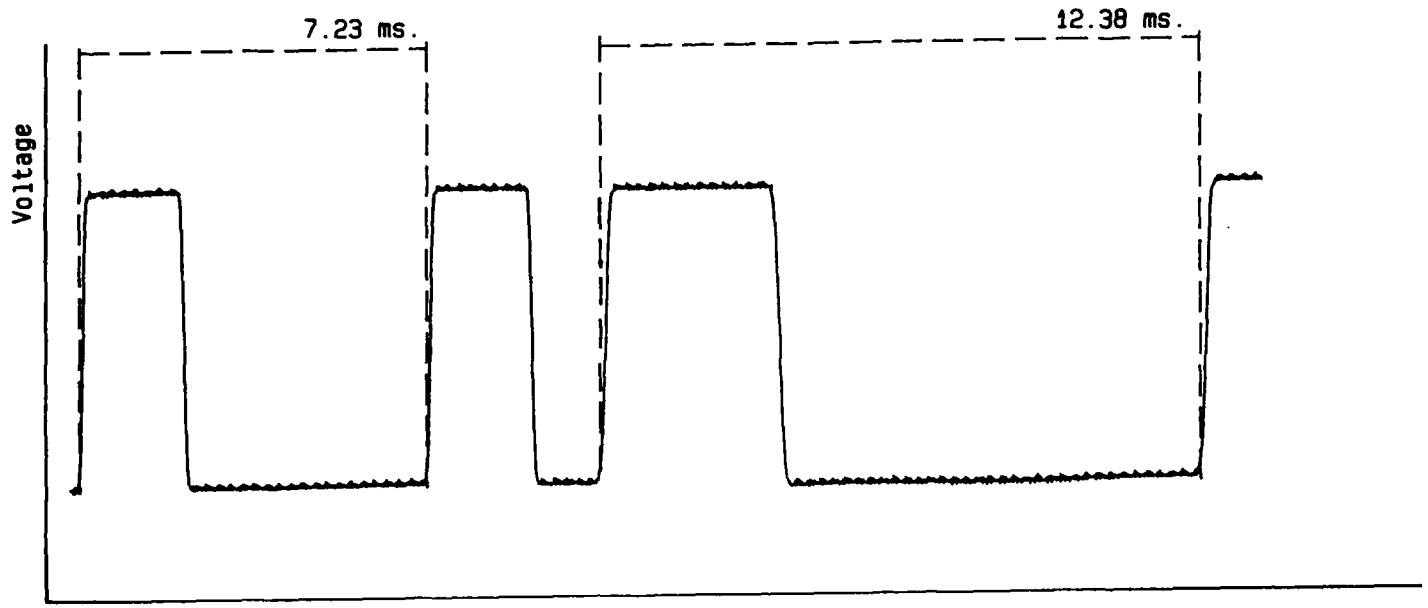

Mass of Impacter	= 1.0000 kg.
Initial time	= 7.2300 ms.
Initial displac.	= 35.1900 mm.
Initial velocity	= 4.8672 m/s.
Initial Energy	= 11.8449 Joules.
Rebound time	= 12.3800 ms.
Rebound displac.	= 35.4600 mm.
Rebound velocity	= 2.8643 m/s.
Rebound Energy	= 4.1021 Joules.
Absorbed Energy	= 7.7428 Joules.

FIG 10: TYPICAL RESULT PLOT FROM AN IMPACT TEST.

FIG 11: TYPICAL C-SCAN OF AN IMPACTED AND DRILLED TEST SPECIMEN.

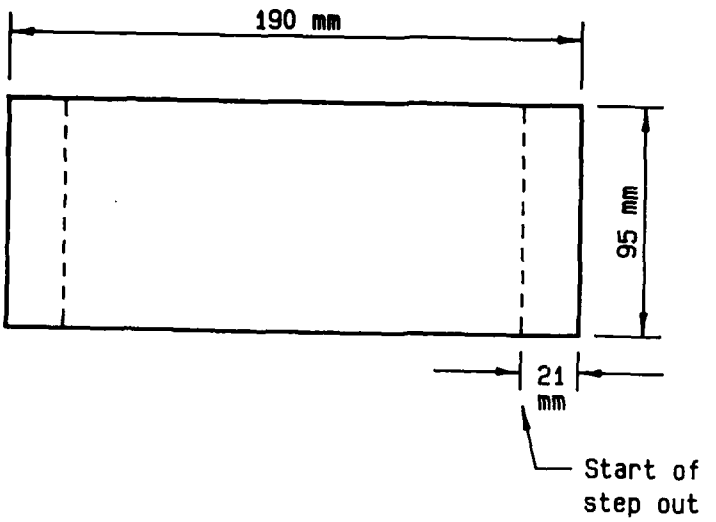

a) Plan view

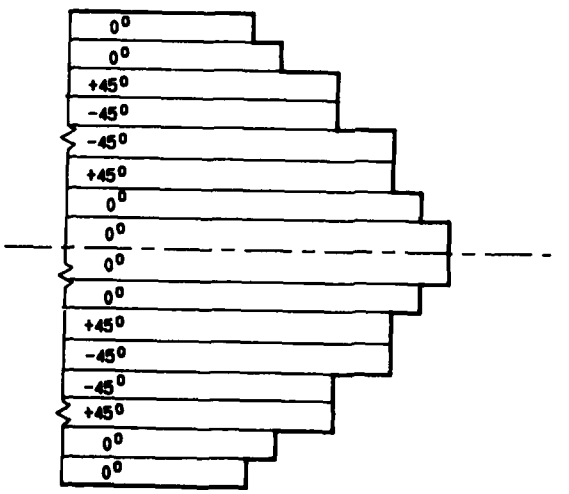

b) Cross section of step out

FIG 12: PATCH DIMENSIONS, LAYUP AND PLY STEP OUT.

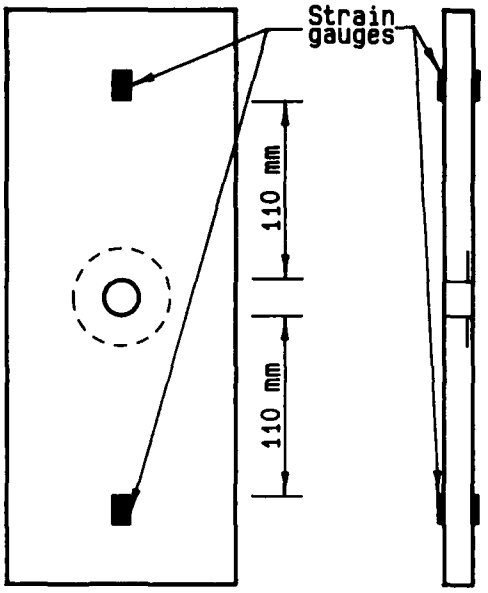

a) Unpatched

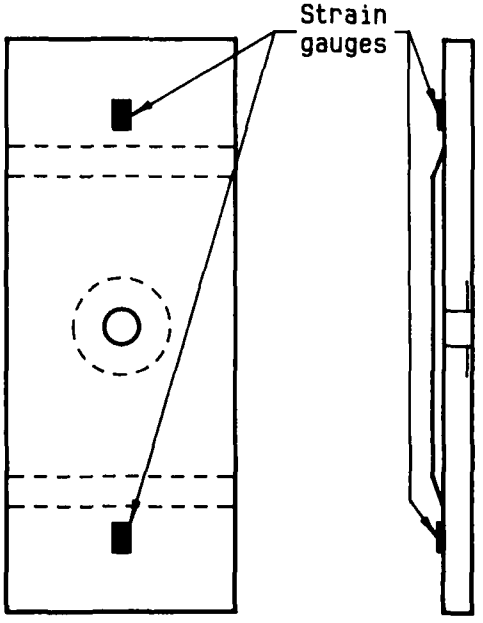

b) Patched

FIG 13: LOCATION OF STRAIN GAUGES ON UNPATCHED AND PATCHED SPECIMENS.

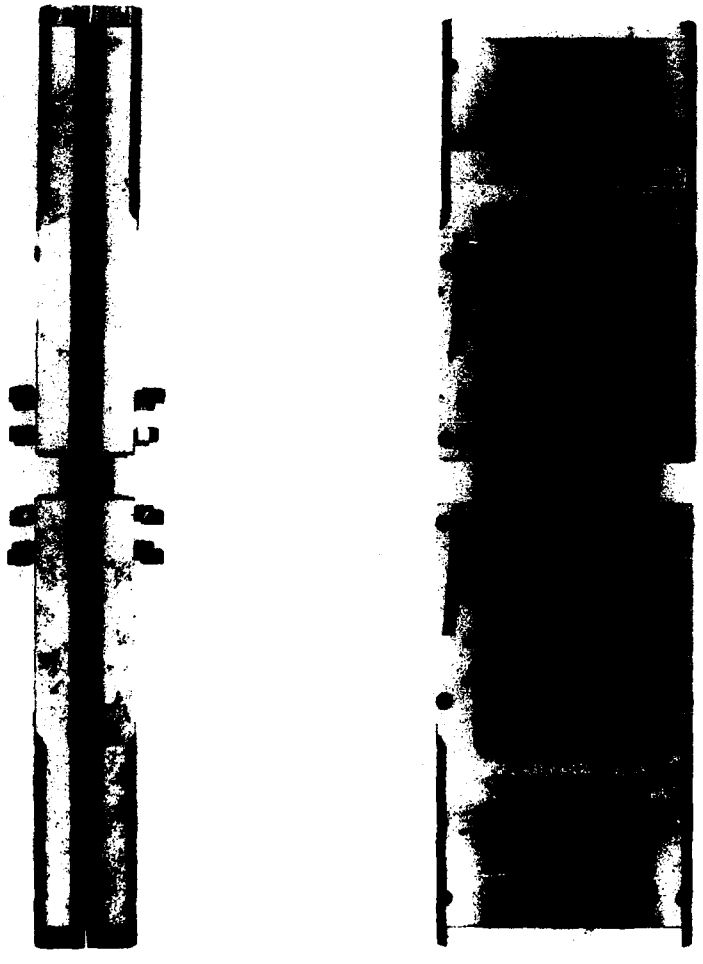

FIG 14: PLAN AND SIDE VIEW OF ANTI-BUCKLING RIG.

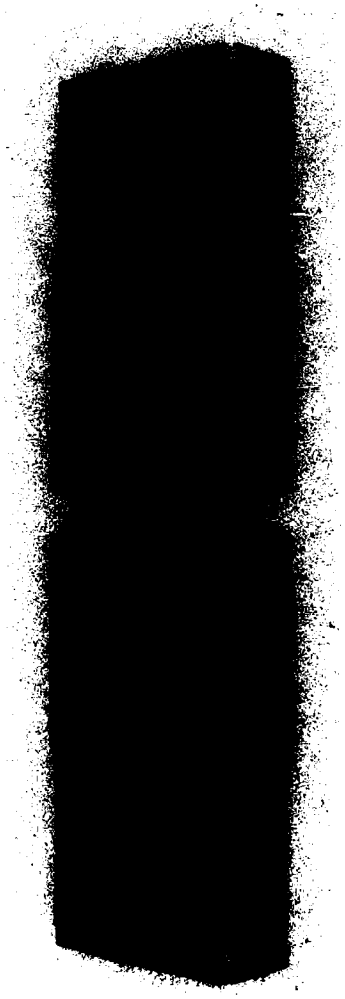

FIG 15: PERSPECTIVE VIEW OF ANTI-BUCKLING RIG.

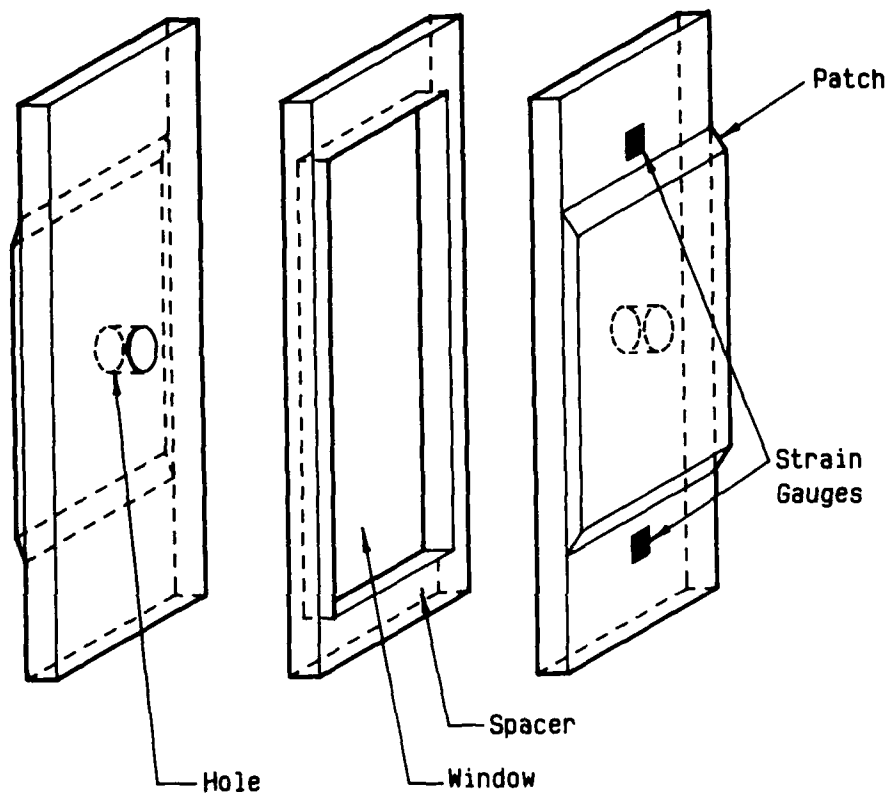

FIG 16: PATCH SPECIMEN TEST CONFIGURATION.

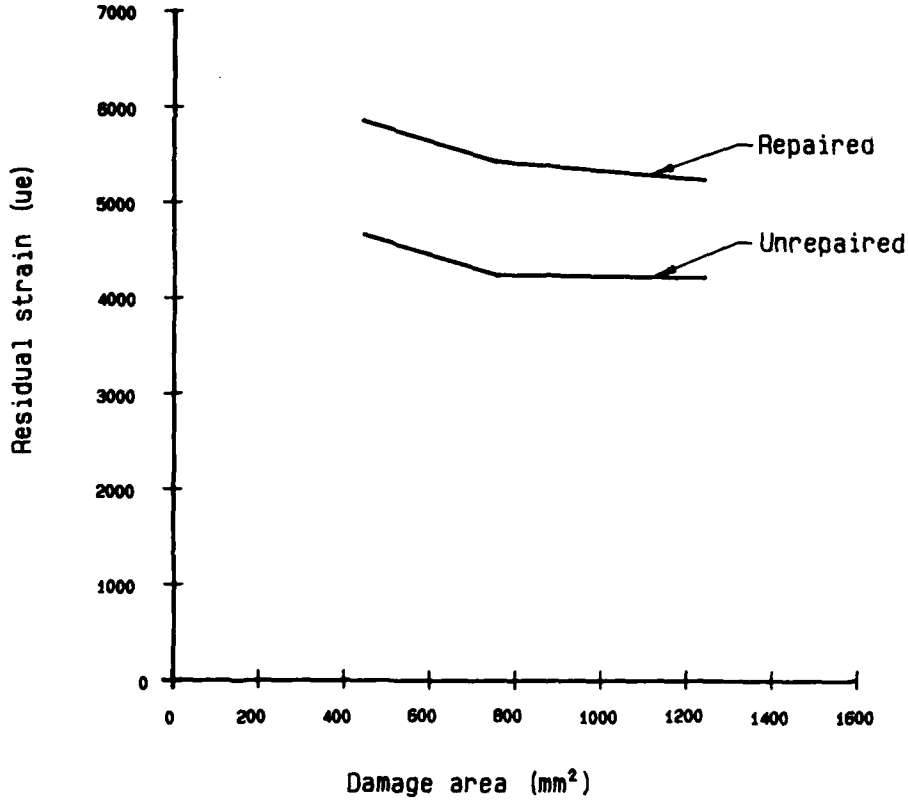

FIG 17: FAILURE STRAIN VERSUS DAMAGE AREA, PLOTTED FROM TEST RESULTS.

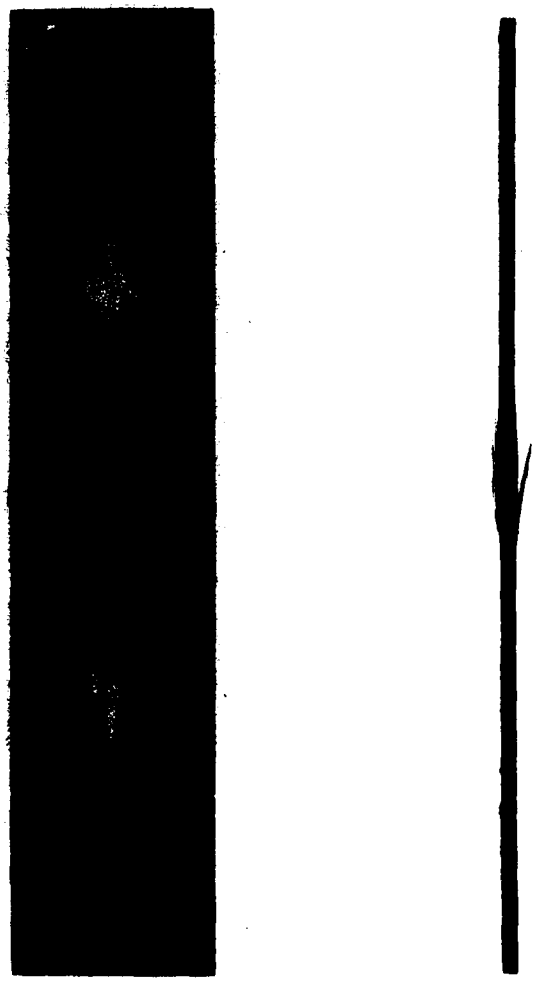

FIG 18: TYPICAL DAMAGE OF AN UNREPAIRED SPECIMEN.

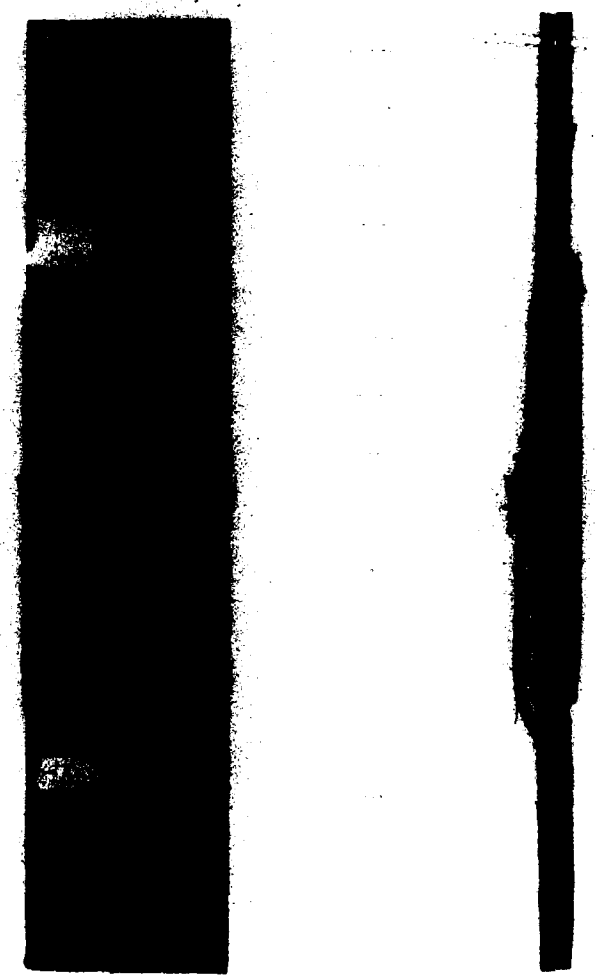

FIG 19: TYPICAL DAMAGE OF A REPAIRED SPECIMEN.

DISTRIBUTION

AUSTRALIA

Department of Defence

Defence Central
- Chief Defence Scientist
- FAS Science Corporate Management (shared copy)
- FAS Science Policy (shared copy)
- Director, Departmental Publications
- Counsellor, Defence Science, London (Doc Data Sheet Only)
- Counsellor, Defence Science, Washington (Doc Data Sheet Only)
- S.A. to Thailand MRD (Doc Data Sheet Only)
- S.A. to the DRC (Kuala Lumpur) (Doc Data Sheet Only)
- OIC TRS, Defence Central Library
- Document Exchange Centre, DISB (18 copies)
- Joint Intelligence Organisation
- Librarian H Block, Victoria Barracks, Melbourne
- Director General - Army Development (NSO) (4 copies)
- Defence Industry and Materiel Policy, FAS

Aeronautical Research Laboratory
- Director
- Library
- Divisional File - Aircraft Structures
- Authors: J. Paul
  R. Jones
- A. Baker
- M. Davis
- L. Molent
- B. Hoskin

Materials Research Laboratory
- Director/Library

Defence Science & Technology Organisation - Salisbury
- Library

Navy Office
- Navy Scientific Adviser (3 copies Doc Data sheet)
- Director of Naval Aircraft Engineering
- Superintendent, Aircraft Maintenance and Repair
- Director of Naval Ship Design

Army Office
- Scientific Adviser - Army (Doc Data sheet only)
- Engineering Development Establishment, Library
- US Army Research, Development and Standardisation Group

Air Force Office
- Air Force Scientific Adviser

Aircraft Research and Development Unit
Scientific Flight Group
Library
Engineering Division Library
Director General Aircraft Engineering - Air Force
Director General Operational Requirements - Air Force
HQ Air Command (SMAINTSO)
HQ Support Command
SLENGO
AIRENG5
AIRENG5A

Department of Transport & Communication
Library

Statutory and State Authorities and Industry
Aero-Space Technologies Australia, Manager/Librarian (2 copies)
Ansett Airlines of Australia, Library
Australian Airlines, Library
Qantas Airways Limited
Civil Aviation Authority
Hawker de Havilland Aust Pty Ltd, Victoria, Library
Hawker de Havilland Aust Pty Ltd, Bankstown, Library
Rolls Royce of Australia Pty Ltd, Manager
BHP, Melbourne Research Laboratories

Universities and Colleges
Adelaide
Barr Smith Library
Professor of Mechanical Engineering

Flinders
Library

LaTrobe
Library

Monash
Hargrave Library
Prof I.J. Polmear, Materials Engineering

Newcastle
Library

Sydney
Engineering Library
Head, School of Civil Engineering

NSW
Physical Sciences Library
Professor R.A. Bryant, Mechanical Engineering
Library, Australian Defence Force Academy

Queensland
Library

Tasmania
Engineering Library

Western Australia
Library
Professor B.J. Stone, Head Mechanical Engineering

RMIT
Library

University College of the Northern Territory
Library

CANADA
CAARC Coordinator Aerodynamics
CAARC Coordinator Structures
International Civil Aviation Organization, Library

NRC
Aeronautical & Mechanical Engineering Library
Division of Mechanical Engineering Library

Universities and Colleges
Toronto
Institute for Aerospace Studies

CZECHOSLOVAKIA
Aeronautical Research and Test Institute (Prague), Head
Czechoslavak Academy of Sciences
Dr J. Helesic

INDIA
CAARC Coordinator Aerodynamics
CAARC Coordinator Materials
CAARC Coordinator Structures
Hindustan Aeronautics Ltd, Library
National Aeronautical Laboratory, Information Centre
Vikram Sarabhai Space Centre, Library

INTERNATIONAL COMMITTEE ON AERONAUTICAL FATIGUE
per Australian ICAF Representative (25 copies)

ISRAEL
Technion-Israel Institute of Technology
Professor J. Singer

ITALY
Professor A. Carpenteri

JAPAN
National Aerospace Laboratory
Professor H. Ishikawa

NETHERLANDS
National Aerospace Laboratory (NLR), Library

NEW ZEALAND

Universities
Canterbury
Library
Professor D. Stevenson, Mechanical Engineering

SINGAPORE
Director, Defence Materials Organisation

SWEDEN
Aeronautical Research Institute, Library

SWITZERLAND
F+W (Swiss Federal Aircraft Factory)

UNITED KINGDOM
Ministry of Defence, Research, Materials and Collaboration
CAARC, Secretary
CAARC Coordinator Aerodynamics

Royal Aircraft Establishment
Farnborough, Dr G. Wood, Materials Department
Commonwealth Air Transport Council Secretariat
National Physical Laboratory, Library
National Engineering Laboratory, Library
British Library, Document Supply Centre
CAARC Co-ordinator, Structures
British Aerospace
Kingston-upon-Thames, Library
Hatfield-Chester Division, Library
Short Brothers Ltd, Technical Library

Universities and Colleges
Bristol
Engineering Library

Cambridge
Library, Engineering Department
Whittle Library

Nottingham
Science Library

Southampton
Library
Fluid Mechanics Division, Dr J.C. Gibbings

Strathclyde
Library

Cranfield Inst. of Technology
Library

Imperial College
Aeronautics Library

UNITED STATES OF AMERICA
NASA Scientific and Technical Information Facility
United Technologies Corporation, Library
Lockheed-California Company
Lockheed Missiles and Space Company
Lockheed Georgia
McDonnell Aircraft Company, Library
Nondestructive Testing Information Analysis Center

Universities and Colleges

Massachusetts Inst. of Technology
MIT Libraries

Spares (10 copies)
Total (170 copies)

AL 149 DEPARTMENT OF DEFENCE

DOCUMENT CONTROL DATA

PAGE CLASSIFICATION
UNCLASSIFIED

PRIVACY MARKING

1a. AR NUMBER	1b. ESTABLISHMENT NUMBER	2. DOCUMENT DATE	3. TASK NUMBER
AR-005-570	ARL-STRUC-R-435	JANUARY 1989	AIR 85/042

4. TITLE
ANALYSIS AND REPAIR OF IMPACT DAMAGED COMPOSITES

5. SECURITY CLASSIFICATION (PLACE APPROPRIATE CLASSIFICATION IN BOX(S) IE. SECRET (S), CONF.(C) RESTRICTED (R), UNCLASSIFIED (U)).

DOCUMENT	TITLE	ABSTRACT
U	U	U

6. NO. PAGES
42

7. NO. REFS.
40

8. AUTHOR(S)
J. PAUL
R. JONES

9. DOWNGRADING/DELIMITING INSTRUCTIONS
NOT APPLICABLE

10. CORPORATE AUTHOR AND ADDRESS

AERONAUTICAL RESEARCH LABORATORY
P.O. BOX 4331, MELBOURNE VIC 3001

11. OFFICE/POSITION RESPONSIBLE FOR:

SPONSOR RAAF
SECURITY -
DOWNGRADING -
APPROVAL DARL

12. SECONDARY DISTRIBUTION (OF THIS DOCUMENT) Approved for public release.

OVERSEAS ENQUIRIES OUTSIDE STATED LIMITATIONS SHOULD BE REFERRED THROUGH ASDIS, DEFENCE INFORMATION SERVICES BRANCH, DEPARTMENT OF DEFENCE, CAMPBELL PARK, CANBERRA, ACT 2601

13a. THIS DOCUMENT MAY BE ANNOUNCED IN CATALOGUES AND AWARENESS SERVICES AVAILABLE TO....
No limitations.

13b. CITATION FOR OTHER PURPOSES (IE. CASUAL ANNOUNCEMENT) MAY BE [X] UNRESTRICTED OR [ ] AS FOR 13a.

14. DESCRIPTORS

Graphite epoxy composites
Impact damage
Repair
Delaminating
Axial compression loads
Australia. (SDW)

15. DRDA SUBJECT CATEGORIES
0071F

16. ABSTRACT

This report discusses the repair of impact damaged graphite/epoxy composite laminates. The behaviour of delamination damage under both uniaxial and biaxial compressive loading is examined and the predictive capabilities of several fracture parameters are investigated. Based upon the results of this analysis a simple repair methodology is proposed and compared with experimental test results.

Keywords.

PAGE CLASSIFICATION UNCLASSIFIED
PRIVACY MARKING

THIS PAGE IS TO BE USED TO RECORD INFORMATION WHICH IS REQUIRED BY THE ESTABLISHMENT FOR ITS OWN USE BUT WHICH WILL NOT BE ADDED TO THE DISTIS DATA UNLESS SPECIFICALLY REQUESTED.

16. ABSTRACT (CONT.)

17. IMPRINT

AERONAUTICAL RESEARCH LABORATORY, MELBOURNE

18. DOCUMENT SERIES AND NUMBER	19. COST CODE COVERED	20. TYPE OF REPORT AND PERIOD
AIRCRAFT STRUCTURES REPORT 435	21 2010	-

21. COMPUTER PROGRAMS USED

PAFEC F.E.

22. ESTABLISHMENT FILE REF.(S)

23. ADDITIONAL INFORMATION (AS REQUIRED)